JOURNAL OF GUIDANCE, CONTROL, AND DYNAMICS
Vol. 33, No. 3, May–June 2010

Solar Sail Three-Body Transfer Trajectory Design

Shengping Gong,* Hexi Baoyin,† and Junfeng Li‡
Tsinghua University, 100084 Beijing, People's Republic of China

DOI: 10.2514/1.46077

This paper discusses design methods of solar sail transfer trajectories in Hill's restricted three-body problem. Based on the premise that the sail attitude is kept fixed with respect to the sunlight, the concepts of the general energy constant and solar sail invariant manifolds are proposed. The invariant manifolds are used to design transfer trajectories from Earth orbits to equilibrium points and trajectories between equilibrium points. Firstly, the general energy constant is employed to evaluate the energy requirement analytically for transfer trajectories from Earth orbits to equilibrium points. It is compared with a direct transfer using a rocket propellant as power source, and eventually the conclusion is reached that a velocity increment of hundreds of meters per second could be saved. For no-impulse transfer trajectories, active control and passive flying stage are incorporated to achieve transfer trajectories. The design problem is converted into a parameter optimization problem, and different objective functions are optimized for comparisons and analysis. The results of comparisons show that the total transfer time is insensitive to different objective functions. Finally, using the symmetry of the dynamical system, the invariant manifolds are patched to develop symmetrical transfer trajectories between symmetrical equilibrium points. Simulations are given for each case to validate the design method.

Nomenclature

$\boldsymbol{a}(a_x, a_y, a_z)$	=	solar radiation pressure acceleration
a_0	=	dimensionless characteristic acceleration
f	=	phase angle describing the spacecraft on a geocentric circular orbit
H	=	orbit altitude of a geocentric orbit
J	=	energy constant for a typical spacecraft
$\tilde{J}$	=	integration constant of a solar sail
$\boldsymbol{n}$	=	unit vector of sail normal direction
R_E	=	radius of the Earth
$\boldsymbol{r}$	=	solar sail position vector
t_a	=	escape time
t_c	=	active control time
t_u	=	flying time on an unstable manifold
t_s	=	flying time on a stable manifold
$\boldsymbol{V}$	=	solar sail velocity vector
$\boldsymbol{V}_n$	=	velocity in the Earth orbit at matching point
$\boldsymbol{v}_s$	=	local stable manifold
$\boldsymbol{v}_u$	=	local unstable manifold
$\boldsymbol{Y}$	=	optimization parameters vector
α	=	cone angle of the sail attitude
α_s	=	cone angle of the sail on a stable manifold
α_u	=	cone angle of the sail on an unstable manifold
θ	=	clock angle of the sail attitude
$\boldsymbol{\lambda}$	=	Lagrange multiplier
μ_E	=	gravitational parameter of the Earth
$\boldsymbol{\Phi}$	=	state constraints at the matching point
ω_E	=	angular velocity of the Earth around the sun

I. Introduction

SOLAR sail is a novel method for space voyaging benefited by propellantless propulsion. Using a solar sail for trajectory transfer is one of the most promising applications in the future. The first modern reference made a detailed investigation of heliocentric spiral trajectories [1]. Other early articles discussed transfers between different heliocentric orbits [2–5]. In recent years, studies of time-optimal trajectories have been performed by a number of authors using both indirect calculus of variations and direct gradient methods, in which the time history of the sail orientation is discretized into segments [6–10]. The sail has to escape from the Earth before it enters a heliocentric orbit. Many reports have discussed the optimal escape trajectories from different Earth orbits [11–14], because Green investigated the escape strategy from a high-altitude Earth orbit in 1977 [15]. Apart from being considered as an ideal space transportation device for some applications, solar sail propulsion has long been considered as a means of enabling special missions. A restricted three-body analysis shows that large sets of new artificial equilibria exist [16]. In the Geostorm mission, a sail working at the sub-L1 artificial Lagrange point is used to advance the warning of geostorms [17,18]. The investigation of the existence and stability of artificial Lagrange points in classical celestial mechanics has been pursued [19]. The dynamics and control of solar sails at artificial Lagrange points are investigated in [20–22]. McInnes proposed a passive control strategy when discussing the control of solar sails on displaced solar orbits, where the sail attitude is kept fixed with respect to the sunlight [23]. This is referred to as passive control, because it can be realized by designing the configuration of the sail, where a four-triangle sail configuration is adopted to make the sail stable on the displaced solar orbits [24]. It was demonstrated by Kirpichnikov that passive stability and flight-path control can be achieved in two-dimensional trajectories by using a sail geometry consisting of two rectangular reflecting surfaces connected at an angle along one edge with the apex pointing toward the sun [25]. The passive flying designs of three-dimensional trajectories inward, toward the sun, and outward are reported in [26,27], where the results indicate that the passive control method using multiple sail surfaces is a promising approach in the search for the best design of propellantless spaceflight systems. In addition, the invariant manifolds exist in the neighborhood of artificial Lagrange points and the center manifolds are used to generate periodic orbits around the points in [28].

In this study, based on the premise that the solar sail can be passively stable, which means that the attitude angles of the sail are kept fixed with respect to the sunlight, the stable and unstable manifolds of artificial Lagrange points were employed to design transfer trajectories. Both the transfer trajectories from Earth orbits to equilibrium points and transfer trajectories between equilibrium points were investigated. Three kinds of Earth orbits to equilibrium points transfer trajectories and three kinds of equilibrium to

Received 21 June 2009; revision received 7 February 2010; accepted for publication 9 February 2010.

*Postdoctoral Fellow, School of Aerospace; gsp04@mails.tsinghua.edu.cn.
†Associate Professor, School of Aerospace; baoyin@tsinghua.edu.cn.
‡Professor, School of Aerospace; lijunf@tsinghua.edu.cn.

equilibrium transfer trajectories are designed. Some transfer trajectories include active control stages and the others include only passive stages. The direct method is used to optimize different objective functions. Comparisons of these results show that the total transfer time is insensitive to objective functions. The transfer trajectory taking the active control time as objective function is the shortest in terms of active control time among all cases. For transfer trajectories between equilibrium points, the symmetry of the dynamical system was used to design symmetrical transfer trajectories between symmetrical equilibrium points. Similarly, the optimization method is also used to solve design problems. Numerical simulations are given to validate the design methods for each case.

II. Hill's Restricted Three-Body Problem

If the motion of the spacecraft is restricted in the vicinity of the Earth, the Hill's restricted three-body problem (Hill's R3BP) can be derived as an approximation of the circular restricted three-body problem. As shown in Fig. 1, the origin is at Earth's mass center; the x axis is along the sun–Earth line; the z axis is along the direction of the angular velocity of the Earth around the sun; and the y axis forms the right-handed triad with the x and z axes. For Hill's R3BP, the solar radiation pressure can be regarded as constant and the sunlight direction is assumed to be along the x axis. The resulting equations of motion can be written as

$$\begin{cases} \ddot{x} - 2\omega_E \dot{y} = 3\omega_E^2 x - \frac{\mu_E x}{r^3} + a_x \\ \ddot{y} + 2\omega_E \dot{x} = -\frac{\mu_E y}{r^3} + a_y \\ \ddot{z} = -\frac{\mu_E z}{r^3} - \omega_E^2 z + a_z \end{cases} \tag{1}$$

where $r = \sqrt{x^2 + y^2 + z^2}$.

A constant sunlight direction and constant characteristic acceleration are assumed here. The model error of solar radiation pressure acceleration magnitude decreases with the distance from the sail to the Earth. Because only the artificial Lagrange points in the vicinity of the Earth are investigated, the acceleration magnitude variation is always less than 0.01%.

The form of the Hill equations of motion allows for the nondimensionalization of the model and elimination of all free parameters. More precisely, by taking $l = \left(\frac{\mu_E}{\omega_E^2}\right)^{1/3}$ as the unit length and $\tau = \frac{1}{\omega_E}$ as the unit time, the equations of motion can be transformed into the following dimensionless equations:

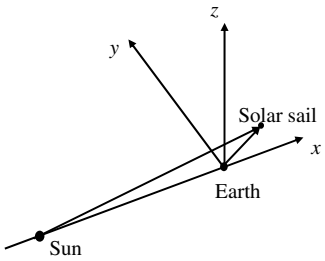

Fig. 1 Schematic geometry of the Hill's restricted three-body problem.

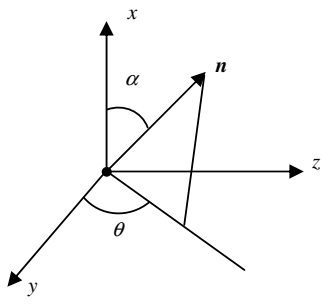

Fig. 2 Description of sail normal in the rotating frame.

Table 1 Dimensionless units

Length, km	Velocity, m/s	Acceleration, m/s^2	Time, day	Characteristic acceleration, mm/s^2
2.1584e6	429.7510	8.5565e − 5	58.1310	0.085398

$$\begin{cases} \ddot{x} - 2\dot{y} = 3x - \frac{x}{r^3} + a_x \\ \ddot{y} + 2\dot{x} = -\frac{y}{r^3} + a_y \\ \ddot{z} = -\frac{z}{r^3} - z + a_z \end{cases} \tag{2}$$

An ideal flat solar sail model is assumed here. The orientation of the solar sail thrust vector is often described in terms of the cone and clock angles. These two angles are the typical trajectory control inputs used in solar sail trajectory optimization. As illustrated in Fig. 2, the orientation of a unit vector normal to the sail plane $\boldsymbol{n}$ is described in terms of the cone angle α and the clock angle θ as follows:

$$\begin{cases} a_x = a_0 \cos^3\alpha \\ a_y = a_0 \cos^2\alpha \sin\alpha \cos\theta \\ a_z = a_0 \cos^2\alpha \sin\alpha \sin\theta \end{cases} \tag{3}$$

The relations between the dimensionless units and units in brackets are presented in Table 1.

For a spacecraft of a negligible area-to-mass ratio (a typical spacecraft), two Lagrange points, L1 and L2, exist for Eq. (2). They are located at $\pm(1/3)^{1/3}$ in dimensionless coordinates. The solar sail can be equilibrated at other points, depending on the characteristic acceleration and attitude of the solar sail. Letting $U = \frac{1}{2}(z^2 - 3x^2) - \frac{1}{r}$, $\boldsymbol{a} = a_0 \cos^2\alpha \boldsymbol{n}$, the stationary solutions in the rotating frame will be generated if the following condition is satisfied:

$$\boldsymbol{a} = \nabla U \tag{4}$$

The vector $\boldsymbol{a}$ should be oriented in the direction of ∇U, so that the required sail orientation is given by

$$\boldsymbol{n} = \frac{\nabla U}{|\nabla U|} \tag{5}$$

The required characteristic acceleration can be obtained as

$$a_0 = \frac{|\nabla U|}{\cos^2\alpha} \tag{6}$$

The region of space in the rotating frame in which stationary solutions exist is bounded, being defined by the region $a_x = 0$. Therefore, the area where the stationary solutions exist can be defined by

$$S(\boldsymbol{r}) = \frac{x}{r^3} - 3x \geq 0 \tag{7}$$

The solution to inequality Eq. (7) can be given by

$$\begin{cases} x \geq 0 \\ r \leq (\frac{1}{3})^{1/3} \end{cases} \quad \text{or} \quad \begin{cases} x \leq 0 \\ r \geq (\frac{1}{3})^{1/3} \end{cases} \tag{8}$$

The solutions exist inside the right hemisphere and outside the left hemisphere with a radius of $(1/3)^{1/3}$. In the xy plane, the solutions exist within the right hemicircle and outside the left hemicircle, as shown in Fig. 3. A section of the surfaces of constant characteristic acceleration a_0 is shown in the figure. It can be seen that the level surfaces around L1 and L2 accessible to the solar sail expand with increased characteristic acceleration, but always contain the classical Lagrange point they are associated with, as this corresponds to the solution $\alpha = \pm\pi/2$. The conclusion accords with that obtained in [15].

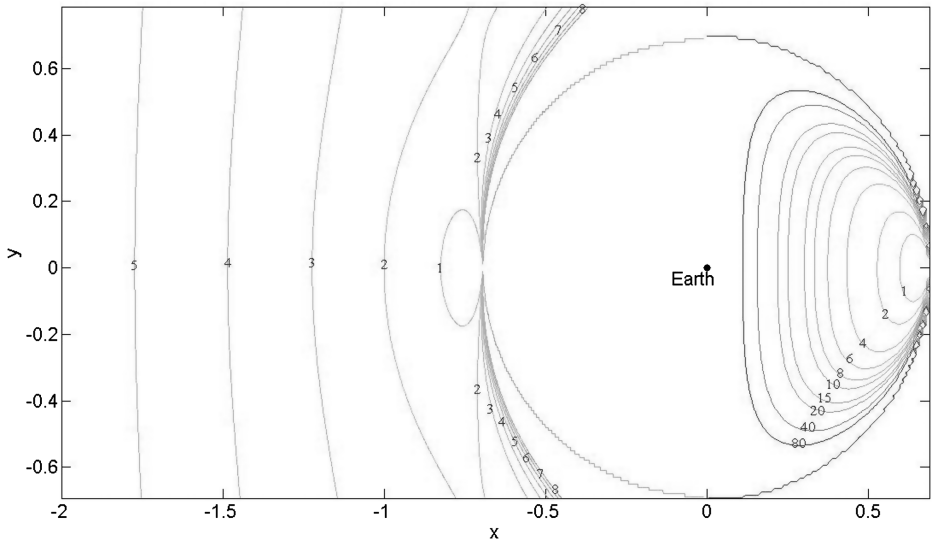

Fig. 3 Characteristic acceleration contour.

For a typical spacecraft, the energy constant exists in Hill's restricted three-body problem:

$$J = \frac{1}{2}(\dot{x}^2 + \dot{y}^2 + \dot{z}^2) + U \tag{9}$$

For a solar sail of constant pitch and clock angles, a new integral constant exists instead of the energy constant. The integral constant can be written as

$$\tilde{J} = \frac{1}{2}(\dot{x}^2 + \dot{y}^2 + \dot{z}^2) + U - a_0\cos^3\alpha x - a_0\cos^2\alpha\sin\alpha\cos\theta y - a_0\cos^2\alpha\sin\alpha\sin\theta z \tag{10}$$

Constant $\tilde{J}$ is named as the general energy of the solar sail. Known from the definition of the general energy, it depends on both the position and sail attitude angles. These two integration constants are used to evaluate the energy required for the transfer from an Earth orbit to an equilibrium point.

III. Invariant Manifolds

The local invariant manifolds of artificial Lagrange points can be calculated based on local dynamical characteristics of artificial Lagrange points. These manifolds can be globalized using a numerical method [29]. The planar case is considered in this paper. In the xy plane, the dynamical equations of motion can be written as

$$\begin{cases} \ddot{x} - 2\dot{y} = 3x - \frac{x}{r^3} + a_0\cos^3\alpha \\ \ddot{y} + 2\dot{x} = -\frac{y}{r^3} + a_0\cos^2\alpha\sin\alpha \end{cases} \tag{11}$$

The characteristic acceleration and attitude for a stationary solution of $\boldsymbol{r}_0 = [\,x_0 \quad y_0\,]^T$ are given by

$$\begin{cases} \tan\alpha_0 = \frac{y_0}{x_0}\frac{r_0^3}{1-r_0^3} \\ a_0 = \frac{1}{\cos^2\alpha}\sqrt{\frac{1}{r_0^4} - 6\frac{x_0^2}{r_0^3} + 9x_0^2} \end{cases} \tag{12}$$

If the cone angle is kept fixed, the dynamical equation in the local neighborhood of $\boldsymbol{r}_0$ is obtained in the usual manner using an arbitrary perturbation $\Delta\boldsymbol{r}$, such that $\boldsymbol{r} = \boldsymbol{r}_0 + \Delta\boldsymbol{r}$. The variational equation is obtained as

$$\begin{bmatrix} \Delta\ddot{x} \\ \Delta\ddot{y} \end{bmatrix} + \begin{bmatrix} 0 & -2 \\ 2 & 0 \end{bmatrix}\begin{bmatrix} \Delta\dot{x} \\ \Delta\dot{y} \end{bmatrix} + \begin{bmatrix} -k_1 & -k_2 \\ -k_2 & -k_4 \end{bmatrix}\begin{bmatrix} \Delta x \\ \Delta y \end{bmatrix} = 0 \tag{13}$$

where $k_1 = \frac{3x_0^2}{r_0^5} + 3 - \frac{1}{r_0^3}$, $k_2 = \frac{3x_0y_0}{r_0^5}$, $k_4 = \frac{3y_0^2}{r_0^5} - \frac{1}{r_0^3}$.

The characteristic equation can be given by

$$\lambda^4 + \left(1 - \frac{1}{r_0^3}\right)\lambda^2 + \left(-\frac{3}{r_0^3} - \frac{2}{r_0^6} + \frac{9y_0^2}{r_0^5}\right) = 0 \tag{14}$$

The eigenvalues and corresponding eigenvectors are dependent on the solar sail parameters. For the equilibrium points in the right half-plane, where $r_0^3 \le 1/3$ is satisfied, the discriminant of the

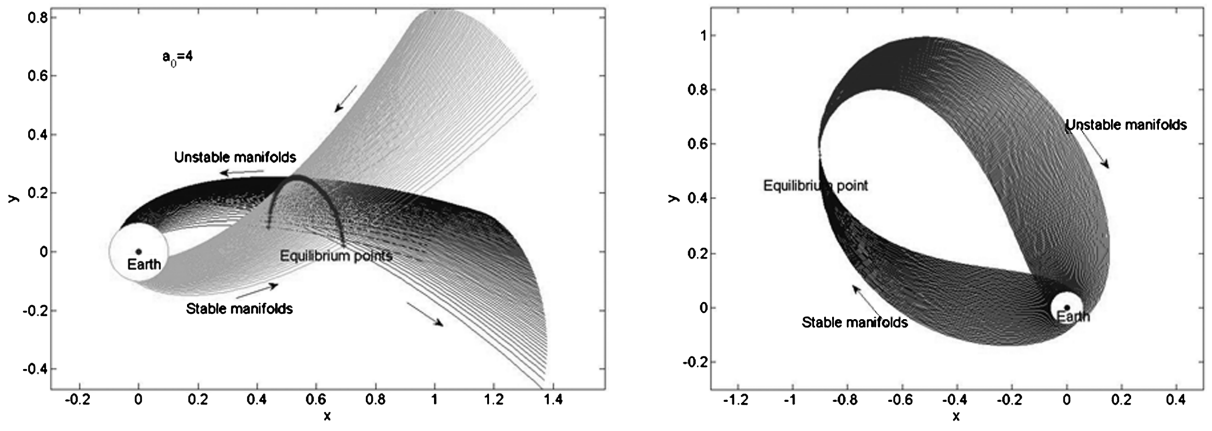

a) Manifolds for different point **b) Manifolds for different cone angles**

Fig. 4 Invariant manifolds for equilibrium points.

characteristic equation is always positive. Therefore, two real roots exist for the equation and they are labeled as $\lambda_{1,2}^2$. Using the relationships between the roots and coefficients, the following conclusions are drawn:

$$\begin{cases} \lambda_1^2 + \lambda_2^2 = \frac{1}{r_0^3} - 1 \geq 0 \\ \lambda_1^2 \cdot \lambda_2^2 = -\frac{3}{r_0^3} - \frac{2}{r_0^6} + \frac{9y_0^2}{r_0^5} \leq 0 \end{cases} \tag{15}$$

It can be concluded that one positive and one negative root exist for the system. Therefore, the fixed points in the xy plane have the linear dynamic properties of saddles and have the linear spectrum

$$(\pm\eta \quad \pm\omega i) \tag{16}$$

where η and ω are two positive numbers.

The structure of the invariant manifolds of a nonlinear system Eq. (11) can be determined from the form of Eq. (16). There is a two-dimensional center manifold upon which trajectories oscillate around the fixed point with a frequency ω [30]. There is one stable and one unstable manifold associated with each fixed point, and they characterize the flow onto and away from the fixed point. The stable and unstable manifolds in the vicinity of the fixed points are determined by the corresponding eigenvectors, which can be given by

$$\upsilon_s = \begin{pmatrix} 1 & \frac{s_2+2\eta}{\eta^2-s_4} & -\eta & -\eta\frac{s_2+2\eta}{\eta^2-s_4} \end{pmatrix} \tag{17}$$

$$\upsilon_s = \begin{pmatrix} 1 & \frac{s_2-2\eta}{\eta^2-s_4} & \eta & \eta\frac{s_2-2\eta}{\eta^2-s_4} \end{pmatrix} \tag{18}$$

where s_2 and s_4 are two real numbers.

Having the local stable and unstable manifolds, the global manifolds are obtained in the following way. Take the stable manifold of the artificial Lagrange point $\boldsymbol{r}_0 = [x_0 \quad y_0]^T$, for example. An initial state on the stable manifold is selected as

$$\boldsymbol{X}_i = [x_0 \quad y_0 \quad 0 \quad 0]^T + \varepsilon \cdot \boldsymbol{\upsilon}_s \tag{19}$$

where ε is selected to guarantee that $\boldsymbol{X}_i$ is in the vicinity of the equilibrium point.

The nonlinear dynamical equation is integrated from the initial state backward in time. The cone angle α_0 can be calculated from Eq. (12). The local manifolds are calculated based on the cone angle α_0. However, the cone angle can be different from α_0 when the manifold is globalized. In this case, an attitude adjustment is required at the matching point of the local and global manifolds. Consequently, the passive cone angle of the solar sail is a free parameter for the globalization of the invariant manifolds.

Figure 4a shows the stable and unstable manifolds for the points requiring the sail characteristic acceleration of 4, that is, $a_0 = 4(0.3416\ \text{mm/s}^2)$. The manifolds are globalized by taking the cone angle equal to α_0. The invariant manifolds of a single point are shown in Fig. 4b, where the manifolds are obtained by globalizing them with different cone angles. The intersection points of the invariant manifolds and a circular Earth orbit are also presented. It can be seen that both the stable and unstable manifolds approach the Earth. Therefore, the stable manifolds can be employed to design transfer trajectories from the Earth orbits to the equilibrium points, and the unstable manifolds can be used to design the trajectories from the equilibrium points back to the Earth. However, the velocity of the sail on the manifolds is different from that of the spacecraft on Earth orbit at the intersection point. Therefore, either an impulse is applied on the Earth orbit or the solar radiation pressure force is used to make the sail enter the stable manifold of the target point.

IV. Transfer Trajectory Design

In this section, two assumptions are made for a deployed solar sail:
1) There is no chemical propulsion system for orbit maneuvers.
2) The attitude can be adjusted for orbit maneuver.

Two categories of transfer trajectories are investigated: transfer trajectories from Earth orbits to equilibrium points and transfer trajectories between equilibrium points. The transfer trajectories may include three different stages: Earth escape stage, active control stage, and passive flying stage.

1) During the Earth escape stage, the solar sail uses solar radiation pressure force to accelerate itself to escape from the Earth. The optimal escape strategies in the two-body problem are investigated in [12–14]. The normal of the solar sail is aligned along the direction in which the energy increases fastest. In the Hill's restricted three-body problem, the derivative of the energy can be given by

$$\dot{J} = \dot{\boldsymbol{V}}^T \boldsymbol{V} - (\nabla U)^T \boldsymbol{V} \tag{20}$$

Equation (20) can be simplified by substituting $\dot{\boldsymbol{V}} = \nabla U + \boldsymbol{a}$ into the expression [12].

$$\dot{J} = \boldsymbol{a}^T \boldsymbol{V} \tag{21}$$

For a planar case, the velocity can be written as $\boldsymbol{V} = V[\cos\tilde{\alpha} \quad \sin\tilde{\alpha}]^T$; then, the energy derivative is given by

$$\dot{J} = \boldsymbol{a}^T \boldsymbol{V} = a_0 V \cos^2\alpha(\cos\alpha\cos\tilde{\alpha} + \sin\alpha\sin\tilde{\alpha}) \tag{22}$$

The optimal cone angle can be obtained by setting $\partial\dot{J}/\partial\alpha = 0$, given by [31]

$$\tan\alpha = \frac{-3 \pm \sqrt{9 + 8\tan^2\tilde{\alpha}}}{4\tan\tilde{\alpha}} \tag{23}$$

The sign in Eq. (23) is taken as the same as that of the velocity of the sail along the x axis. Therefore, the optimal control law during the first stage can be given by

$$\begin{cases} \tan\alpha = \frac{-3+\sqrt{9+8\tan^2\tilde{\alpha}}}{4\tan\tilde{\alpha}}, & \dot{x} > 0 \\ \tan\alpha = \frac{-3-\sqrt{9+8\tan^2\tilde{\alpha}}}{4\tan\tilde{\alpha}}, & \dot{x} \leq 0 \end{cases} \tag{24}$$

2) During the active control stage, the cone angle of the sail is adjusted to control the sail to achieve the desired orbit.

3) During the passive flying stage, the sail flies along the invariant manifolds of equilibrium points and the sail cone angles are kept fixed with respect to the rotating frame.

The design problem is converted into a parameter optimization problem. The active control stage is divided into several segments and the cone angle is kept fixed during each segment. Different stages are incorporated to form a parameter optimization problem. This method can avoid the difficulty of solving a two-point boundary problem that occurs in the indirect method. In principle, this seems a disadvantageous approach because the steering law will not be a good approximation to the true optimal steering law. In fact, the discrete control law provides a good approximation of the true optimal law, especially for a proper number of discrete segments [9].

A. E-A Transfer Trajectories (Earth Orbits to Artificial Lagrange Points)

For transfer trajectories from Earth orbits to the equilibrium point, three different trajectories are discussed, as shown in Fig. 5.

1) E-A-I: An impulse is exerted on the sail to insert the sail into the stable manifold of the target point before the sail deployment. No Earth escape stage is required and the transfer time can be reduced greatly.

2) E-A-II: To save energy, the sail can be deployed on an Earth orbit and the solar radiation pressure force is used for Earth escape. After escape, an active control stage is used to insert the sail into the stable manifold of the target point. Then, the sail flies to the target point along the stable manifold. To reduce the control effort, the active control time should be as short as allowed. There is a special case where no active stage exists. The sail enters the stable manifold of the target point after escaping from the Earth.

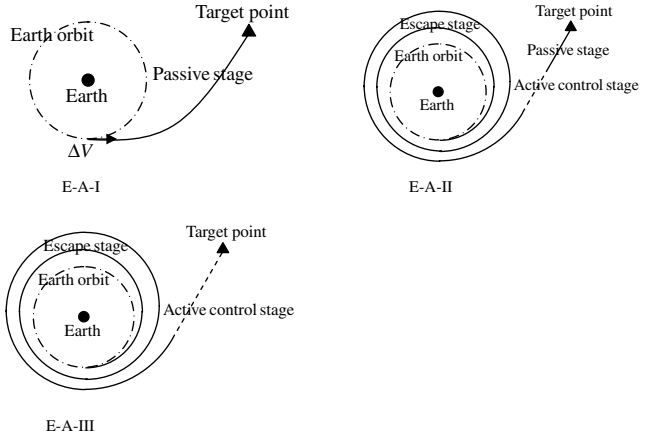

Fig. 5 Illustrations of three different E-A transfer trajectories.

3) E-A-III: After escape, the active control is used to guide the sail to the target point directly. The transfer trajectory does not include passive flying stage. The transfer time during the active control stage is minimized. This kind of transfer trajectory is compared with the E-A-II transfer trajectory.

The E-A-II and E-A-III transfer trajectories include two phases: the escape phase and the transfer phase from the escape orbit to the target point. The Earth escape strategies for solar sailing have been investigated by several authors [12–14], and their results show that the local optimal control law generates a near minimum-time escape strategy, which means that a minimum-time transfer phase from the escape orbit to the target point will lead to a near minimum-time mission trajectory. Therefore, we only need to design the minimum-time transfer trajectory from the escape orbit to the target point. The time-optimal interplanetary trajectory transfers using solar sails have been investigated by different authors [8,10]. The direct method discussed in the references is employed to solve the transfer trajectory design problem here.

The following case is discussed: the spacecraft is launched into a circular Earth orbit of altitude H. The target point of the mission is an artificial Lagrange point $\boldsymbol{r}_0 = [\,x_0 \quad y_0\,]^T$ and the sail cone angle at the point is α_0. A characteristic acceleration of a_0 of the sail is used to achieve the transfer trajectory.

1. E-A-I Transfer Trajectory Design

For this transfer strategy, the key issue is to minimize the energy required to insert the sail into the stable manifold of the target point. If the required impulse cost is too high, it is impractical or inefficient for engineering. The merit of the strategy is that no active control is required during the transfer journey from the escaped orbit to the target point. The objective of the trajectory design is to reduce the impulse cost as much as allowed. The impulse at the circular orbit can be evaluated through an analytical method. If the solar sail flies to the target point at a cone angle α_s, the general energy constant of the sail on the transfer trajectory can be written as

$$\tilde{J}_t = \left(-\frac{1}{r_0} - \frac{3}{2}x_0^2 - a_0\cos^3\alpha_s x_0 - a_0\cos^2\alpha_s \sin\alpha_s y_0\right) \tag{25}$$

where $R = R_E + H$ is the geocentric distance of the sail.

Assuming the coordinate at the intersection point is $(\,x_p \quad y_p\,)$, the general energy of the sail on the circular orbit at the intersection point is given by

$$\tilde{J}_n = -\frac{1}{R} - \frac{3}{2}x_p^2 - a_0\cos^3\alpha_s x_p - a_0\cos^2\alpha_s \sin\alpha_s y_p + \frac{V_n^2}{2} \tag{26}$$

where V_n is the velocity of the spacecraft on the circular orbit.

If the polar coordinates are used to describe the intersection position, then we have $x_p = R\cos f$ and $y_p = R\sin f$. The general energy difference between the transfer trajectory and circular orbit is obtained as

$$\begin{aligned}\Delta\tilde{J} = \tilde{J}_t - \tilde{J}_n = &\left(-\frac{1}{r_0} - \frac{3}{2}x_0^2 - a_0\cos^3\alpha_s x_0 - a_0\cos^2\alpha_s \sin\alpha_s y_0\right)\\ &+ \left(\frac{1}{2R} + \frac{3}{2}R^2\cos^2 f + a_0\cos^3\alpha_s R\cos f\right.\\ &\left.+ a_0\cos^2\alpha_s \sin\alpha_s R\sin f\right)\end{aligned} \tag{27}$$

The difference is determined by the cone angle α_s and the polar angle of the intersection point f. Actually, the polar angle is determined by the cone angle, which means that there is only one free parameter in the expression of the general energy difference. To analyze the theoretical minimum of the difference, the two parameters can be regarded as free parameters. The minimum can be obtained by differentiating $\Delta\tilde{J}$ with respect to α_s and f:

$$\begin{aligned}\frac{\partial\Delta\tilde{J}}{\partial\alpha_s} = &\,3a_0\cos^2\alpha_s \sin\alpha_s(x_0 - R\cos f) + (2a_0\cos\alpha_s\sin^2\alpha_s\\ &- a_0\cos^3\alpha_s)(y_0 - R\sin f) = 0\end{aligned} \tag{28}$$

$$\begin{aligned}\frac{\partial\Delta\tilde{J}}{\partial f} = &\,3R^2\cos f\sin f + a_0\cos^3\alpha_s R\sin f\\ &- a_0\cos^2\alpha_s \sin\alpha_s R\cos f = 0\end{aligned} \tag{29}$$

The parameters minimizing $\Delta\tilde{J}$ can be solved from the two equations with the consideration of $-\pi/2 \le \alpha_s \le \pi/2$. The numerical method should be employed because the two equations are too complex for analytical methods. To avoid the numerical solution, the general energy difference can be simplified by discarding small numbers. For circular Earth orbits, the radius R is very small in dimensionless units. Therefore, the general energy can be approximated as $\tilde{J}_n = -\frac{1}{2R}$, which is the same as the energy of a typical spacecraft in a two-body problem. This approximation is reasonable, because the gravity of the Earth is dominant near the Earth. Consequently, the difference can be rewritten as

$$\Delta\tilde{J} = \left(-\frac{1}{r_0} - \frac{3}{2}x_0^2 - a_0\cos^3\alpha_s x_0 - a_0\cos^2\alpha_s \sin\alpha_s y_0\right) + \frac{1}{2R} \tag{30}$$

The general energy difference is induced by the velocity difference at the intersection point:

$$\frac{1}{2}V_t^2 - \frac{1}{2}V_n^2 = \Delta\tilde{J} \tag{31}$$

The velocity of the sail at the intersection on the transfer trajectory can be obtained as

$$\begin{aligned}V_t &= \sqrt{2\Delta\tilde{J} + V_n^2}\\ &= \sqrt{2\left(-\frac{1}{r_0} - \frac{3}{2}x_0^2 - a_0\cos^3\alpha_s x_0 - a_0\cos^2\alpha_s \sin\alpha_s y_0 + \frac{1}{R}\right)}\end{aligned} \tag{32}$$

The impulse to compensate for the velocity difference is given by

$$\begin{aligned}\Delta V = |\boldsymbol{V}_n - \boldsymbol{V}_t| &= \sqrt{V_n^2 + V_t^2 - 2V_n V_t\cos\phi} \ge V_n - V_t\\ &= \sqrt{2\left(-\frac{1}{r_0} - \frac{3}{2}x_0^2 - a_0\cos^3\alpha_s x_0 - a_0\cos^2\alpha_s \sin\alpha_s y_0 + \frac{1}{R}\right)}\\ &\quad - \sqrt{\frac{1}{R}}\end{aligned} \tag{33}$$

where ϕ is the angle between $\boldsymbol{V}_n$ and $\boldsymbol{V}_t$, and the minimal impulse is reached if the directions of $\boldsymbol{V}_n$ and $\boldsymbol{V}_t$ coincide with each other.

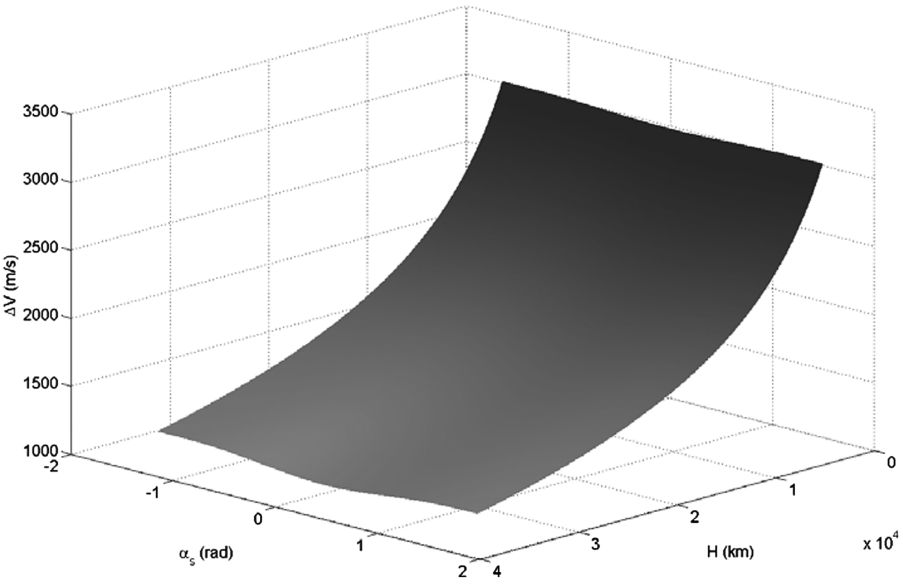

Fig. 6 Velocity increment for different cone angles and circular orbits.

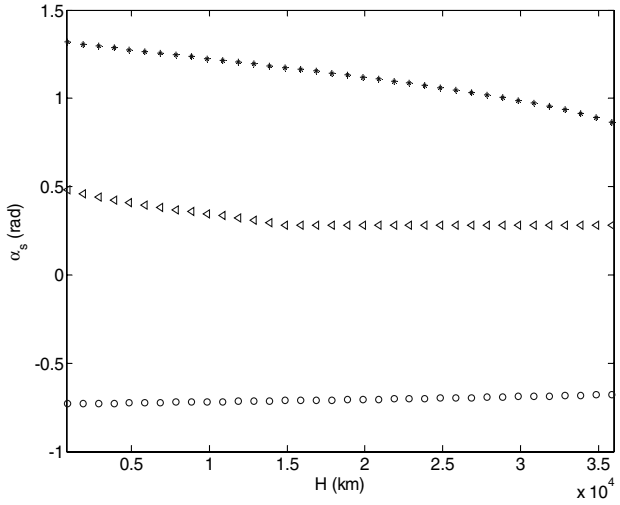

a) Cone angle

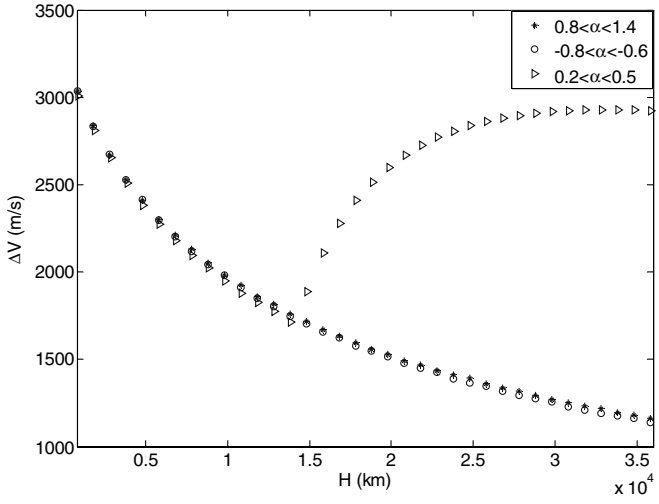

b) Velocity increment

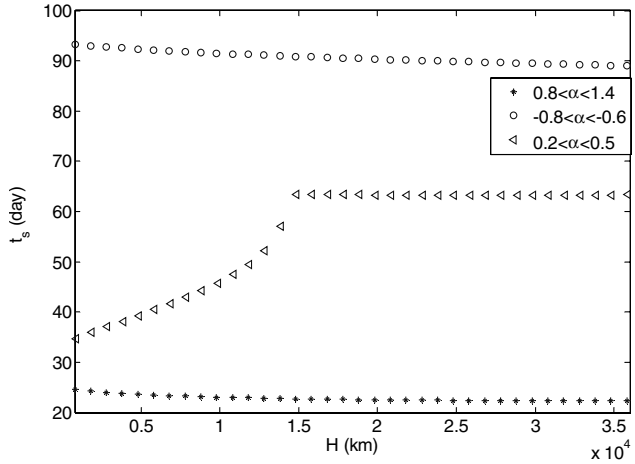

c) Transfer time

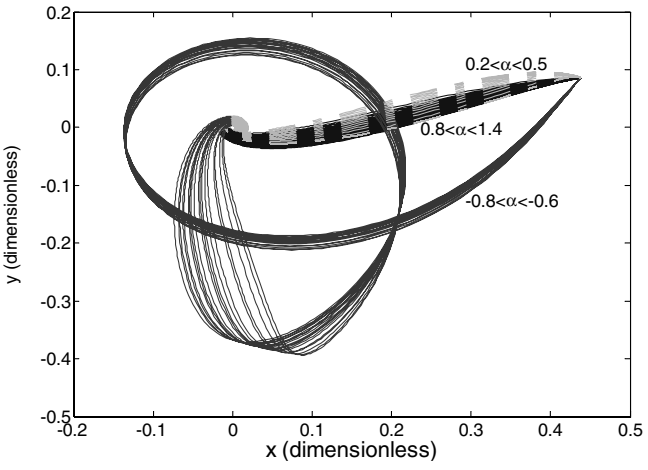

d) Transfer trajectories

Fig. 7 Transfer parameters for different circular altitudes.

Figure 6 gives the theoretical minimal impulse for different orbits and cone angles. It can be seen that the cone angle does not change the minimal impulse much. Therefore, the coincidence of velocity directions is very important to obtain a small impulse.

The minimal impulse was analyzed above, and a numerical method was used to validate the analytical results. Both $\boldsymbol{V}_t$ and the position of the intersection point are determined by the cone angle α_s and the orbit altitude H. Therefore, the impulse is a function of both α_s and H, which can be written as

$$\Delta V = |\boldsymbol{V}_n - \boldsymbol{V}_t| = F(\alpha_s, H) \tag{34}$$

The impulse ΔV can be minimized for a given altitude. A numerical example is given here to analyze the minimal impulse required for different altitudes. The characteristic acceleration of the sail is $a_0 = 4$ ($0.3416\ \text{mm/s}^2$), and it can equilibrate at the target point $\boldsymbol{r}_0 = [0.43818 \quad 0.08541756]^T$ when the cone angle is $\alpha_0 = 0.2599$ rad. For different orbital altitudes, cone angles in three regions generate stable manifolds that have intersection points with the circular orbits. In each region, the impulse is minimized with respect to the cone angle. Figure 7a gives the optimal cone angles for altitudes from 800 to 36,000 km, and the optimal cone angles are within regions (−0.8 −0.6), (0.2 0.5), and (0.8 1.4) rad, respectively. The optimal impulse and corresponding transfer time in each region are given in Figs. 7b and 7c, respectively. In the regions (−0.8 −0.6) and (0.8 1.4) rad, the impulse decreases with the altitude, and the optimal impulses in the two regions are very close, with the impulse in region (−0.8 −0.6) rad a little smaller. The results in region (0.2 0.5) rad are special; the optimal impulses obey the rule of decreasing with the altitude when the altitude is low, but disobey the rule as the altitude exceeds a certain value. The optimal impulse is also the smallest among the three regions for low orbits, which can be seen in Fig. 7b. This happens because the angle between $\boldsymbol{V}_n$ and $\boldsymbol{V}_t$ in this region is always large for high-altitude orbits. Figure 7c shows that the transfer times in different regions are different. The region (0.8 1.4) rad requires a transfer time less than 25 days. The (−0.8 −0.6) rad region requires more than 90 days, and the (0.2 0.5) rad region requires a transfer time between 25 and 90 days.

As we know, the optimizations of time and energy always conflict with each other, and time reduction usually leads to energy increment and vice versa. However, the conflict here is not very obvious. The energy is nearly the same for the three regions, at least for low altitude, but the time is widely divergent. The whole transfer trajectories in Fig. 7d may explain why this happens. Directions of $\boldsymbol{V}_n$ and $\boldsymbol{V}_t$ being close to each other is a key factor in the reduction of the impulse. To make this happen, trajectories have to circle the Earth to seek the right intersection points, which wastes a great deal of time. From the point of view of energy, the optimal impulse required for the transfer can not be reduced too much because of the energy difference between the target point and circular orbit. With the consideration of time and energy, the cone angles in region (0.8 1.4) rad are better. However, a large cone angle maneuver has to be implemented before the sail is inserted into the equilibrium point, because cone angles in this region are much larger than the angle at the equilibrium point $\alpha_0 = 0.2599$ rad. Therefore, the (0.2 0.5) rad region can be used when the altitude is low, with the consideration of attitude adjustment.

For a given orbit altitude, the minimal velocity increment required by the manifold method can be obtained. The theoretical minimum considering the general energy difference can be calculated from Eq. (33). The comparison between the two results is given in Fig. 8. For low altitude, the numerical and analytical results are very close. It means that the impulse vector and velocity vector of the spacecraft on Earth orbit are always close to each other.

The Geostorm mission uses a solar sail to work at a sub-L1 point for geostorm warning. The energy required to transfer the spacecraft from the Earth orbit to the target point can be evaluated for both typical spacecraft and solar sail. The energy requirements are compared for both cases. The energy constant exists for a typical spacecraft and the energy requirement is to compensate for the

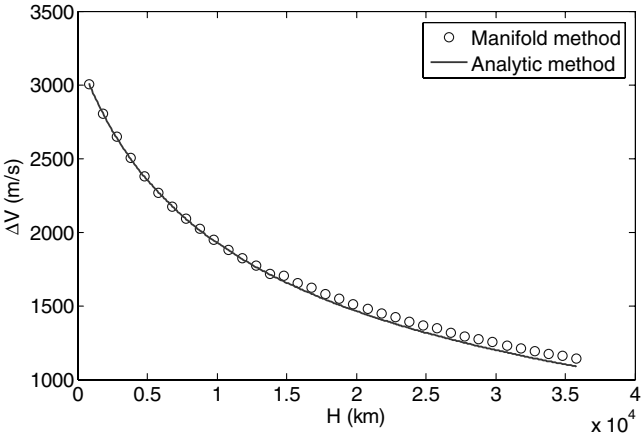

Fig. 8 Minimal velocity increments for different methods.

energy difference between the target point and Earth circular orbit. Similarly, the energy difference can be given by

$$\Delta J = J_t - J_n = \left(-\frac{1}{r_0} - \frac{3}{2}x_0^2\right) - \left(-\frac{1}{2R} - \frac{3}{2}R^2\cos^2 f\right) \tag{35}$$

The energy saved for solar sail transportation is the difference between ΔJ and $\Delta\tilde{J}$, given by

$$\begin{aligned}\Delta J_s = \Delta J - \Delta\tilde{J} &= a_0\cos^3\alpha_s x_0 + a_0\cos^2\alpha_s \sin\alpha_s y_0 \\ &\quad - a_0\cos^3\alpha_s R\cos f - a_0\cos^2\alpha_s \sin\alpha_s R\sin f\end{aligned} \tag{36}$$

To arrive at the target point, the minimal departing velocity for the direct transfer is given by

$$V_t = \sqrt{2\Delta J + V_n^2} = \sqrt{2\left(\frac{1}{R} - \frac{1}{r_0} - \frac{3}{2}x_0^2\right)} \tag{37}$$

The minimal velocity increment at the circular orbit is obtained if it is applied along the direction of circular orbit, which can be written as

$$\Delta V = V_n - V_t = \sqrt{2\left(\frac{1}{R} - \frac{1}{r_0} - \frac{3}{2}x_0^2\right)} - \sqrt{\frac{1}{R}} \tag{38}$$

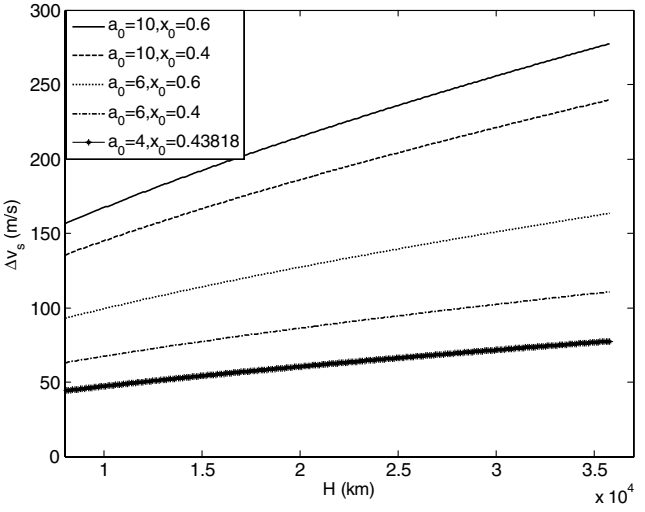

Fig. 9 Velocity increment saved for different target points.

Combination of Eqs. (33) and (38) generates the velocity increment saved at the departing points:

$$\Delta v_s = \sqrt{2\left(\frac{1}{R}-\frac{1}{r_0}-\frac{3}{2}x_0^2\right)} - \sqrt{2\left(\frac{1}{R}-\frac{1}{r_0}-\frac{3}{2}x_0^2-a_0\cos^3\alpha_s x_0-a_0\cos^2\alpha_s\sin\alpha_s y_0\right)} \quad (39)$$

The maximal value of the saved velocity increment is easily obtained from Eq. (39). The characteristic acceleration of the sail is determined by the target point. It can be concluded that the velocity increment saved depends only on the target points. Figure 9 gives the velocity increment saved from different circular orbits to different target points. For the points that are far from the Earth, the solar sail transfer methods can save hundreds of meters per second velocity increment. Therefore, for near-Earth artificial Lagrange point missions, direct transfer is favorable to solar sail transfer with the consideration of safety and reliability. However, the solar sail transfer is much superior for far points with respect to energy consumption.

2. *E-A-II Transfer Trajectory Design*

Solar sails can be used for propellantless propulsion, which is the reason Tsiolkovsky proposed it about a century ago and also why it is still in favor today. For E-A-II transfer trajectories, the solar radiation pressure force is used to escape from the Earth, and the local optimal escape strategy is employed to generate the escape control law. There are two free parameters for the escape stage: the position of the sail deployment on the Earth orbit that is described by f, and the escape time t_a. For the active control stage, the trajectory is discretized into n segments. The design parameters are cone angles during each segment $\alpha_i (i = 1 \ldots n)$ and the time span of this stage t_c. The passive flying stage has two parameters: the cone angle α_s and the flying time t_s. This stage is integrated backward in time from the local stable manifold of the target equilibrium point. The final states of the active control stage and passive flying stage match at a point on the stable manifold. The defect of the two states at the matching point being zero is the constraint $\boldsymbol{\Phi} = 0$. The optimization parameters of the problem are given by [9]

$$\boldsymbol{Y} = [f \quad t_a \quad \alpha_1 \quad \ldots \quad \alpha_n \quad t_c \quad \alpha_s \quad t_s]^T \quad (40)$$

The constraint at the matching point is given by

$$\boldsymbol{\Phi}(\boldsymbol{Y}) = 0 \quad (41)$$

Two kinds of objective functions are chosen to solve the transfer trajectory problem, the time span of the active control stage for the first kind and the total transfer time for the second kind, given by

$$F_{\text{obj}} = t_c \quad (42)$$

$$F_{\text{obj}} = t_c + t_s \quad (43)$$

The augmented Lagrange method is used to convert the constrained optimization problem into an unconstrained one [31]. The objective function for the unconstrained optimization problem can be written as

$$F'_{\text{obj}} = F_{\text{obj}} + \boldsymbol{\lambda}^T \boldsymbol{\Phi}(Y) + \frac{1}{2} c |\boldsymbol{\Phi}(Y)|^2 \quad (44)$$

where c is a positive number.

If the result of the kth optimization is $\boldsymbol{Y}_k$ and the corresponding Lagrange multiplier is $\boldsymbol{\lambda}_k$, the Lagrange multiplier for the next optimization can be taken as

$$\boldsymbol{\lambda}_{k+1} = \boldsymbol{\lambda}_k + \boldsymbol{\Phi} c(Y_k) \quad (45)$$

The special case is that the transfer trajectory includes only two stages: the escape stage and the passive flying stage. The sail enters the stable manifold after the escape stage. The final state of the escape stage and the initial state of the passive flying stage match at a point. The matching defect being zero is the constraint of the optimization problem. In this case, the trajectory design parameters can be given by

Table 2 Design parameters for the no active stage of E-A-II transfer trajectory

Design parameters	Value
Escape time, day	255.0120
Passive flying time, day	11.3169
Cone angle, rad	−0.8908
Position error at matching point, m	223.5
Velocity error at matching point, m/s	5.3e − 5

$$\boldsymbol{Y} = [f \quad t_a \quad \alpha_s \quad t_s]^T \quad (46)$$

The form of the constraint can be described by Eq. (41), which includes four equation constraints, two for position and two for velocity. Therefore, the number of free parameters is the same as the number of constraints. It is more appropriate to describe the problem as algebraic nonlinear equation solving than parameter optimization, because there is no space for optimization. The optimization process is used here because the violation of the constraints is allowed and the value of violation is suppressed, keeping it as small as allowed. Similarly, either the constrained optimization problem or nonlinear equation solving is converted into an unconstrained optimization problem.

3. *E-A-III Transfer Trajectory Design*

Similarly, the active stage is discretized and the attitude during each segment is kept fixed. The sail is guided to the target point directly and no passive stage is used here. The whole trajectory is integrated forward in time and the state error of the sail at the target point being zero is the constraint. To compare different methods, the E-A-II and E-A-III transfer trajectories are designed with the same condition. Therefore, the initial point and the target point are the same with those of the E-A-II transfer trajectory. Only the control time and attitude history are designed here. The optimization parameter vector is given by

$$\boldsymbol{Y} = [\alpha_1 \quad \ldots \quad \alpha_n \quad t_c]^T \quad (47)$$

The constraint and objective function are given by Eqs. (41) and (42), respectively.

4. *Simulations*

A solar sail of characteristic acceleration $a_0 = 4$ (0.3416 mm/s^2) is used to achieve a mission at the target point $\boldsymbol{r}_0 = [0.43818 \quad 0.08541756]^T$. The sail is in the geosynchronous orbit at the initial time. Different cases of transfer trajectories are designed here. The simulations are conduct in the following way:

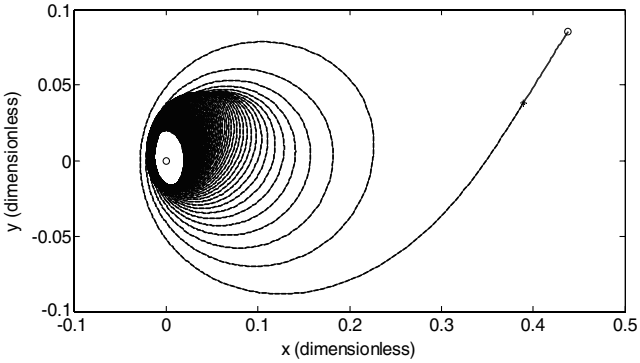

Fig. 10 Transfer trajectory for special case of E-A-II.

1) First, the transfer trajectory including only the escape stage and the passive flying stage, labeled as E-A-II special case, is designed. The optimized sail deployment position is at a polar angle of $f = 3.5643$ rad. After sail deployment, it takes the sail about 4.3868 dimensionless time (255.0120 days) to enter the passive flying stage. During the passive flying stage, the sail flies along the stable manifold with a cone angle of -0.8908 rad and arrives at the target equilibrium point after 0.1947 dimensionless time (11.3169 days). The position and velocity errors at the matching point are very small. The values of the design parameters in the international system of units are given in Table 2. The whole transfer trajectory is shown in Fig. 10.

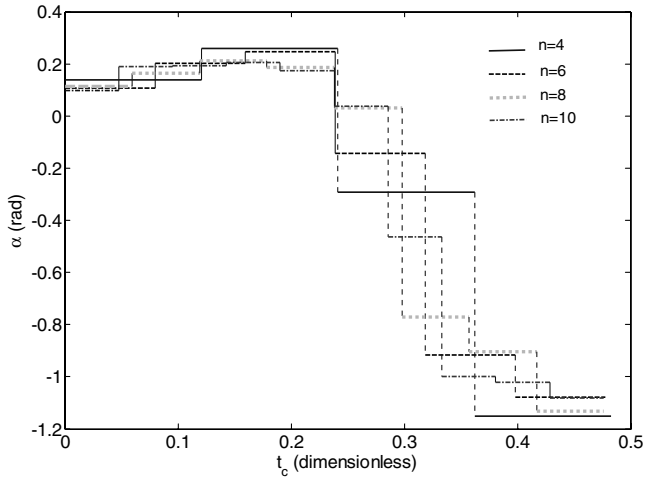

Fig. 11 Control law of E-A-III transfer trajectories.

2) The E-A-III and general cases of E-A-II transfer trajectories are designed. To compare the results of different methods, the sail is deployed at the same point for different methods, $f = 3.5643$ rad. After deployment, the sail flies 4.1 dimensionless time (238.3373 days) to a point in the final loop of the escape trajectory, which is selected to be the start point of the transfer phase from the escaped orbit to the target point. Therefore, the design problem of the whole transfer trajectory turns into a design problem of transfer trajectory between two fixed points. Three cases of transfer trajectories are designed here: two cases of E-A-II transfer trajectories minimizing t_c and $t_c + t_s$, respectively, and one case of E-A-III transfer trajectory. All the transfer trajectories include an active control stage that is discretized into segments. To investigate the influence of the number of the discrete segments on the optimization objective function, the optimized results of different segments are presented. Usually, a small number of segments cannot generate good results, and a large number requires more attitude maneuvers. Therefore, the number of segments should be chosen properly to make the active control time close to true minimum but not too large for operation. The optimized results of three cases are shown in Figs. 11–13, respectively. The position defect is less than 10 m and velocity defect is less than 1 m/s for each optimization.

For the E-A-III transfer trajectories, active control is used during the whole journey. A near minimum-time transfer trajectory is

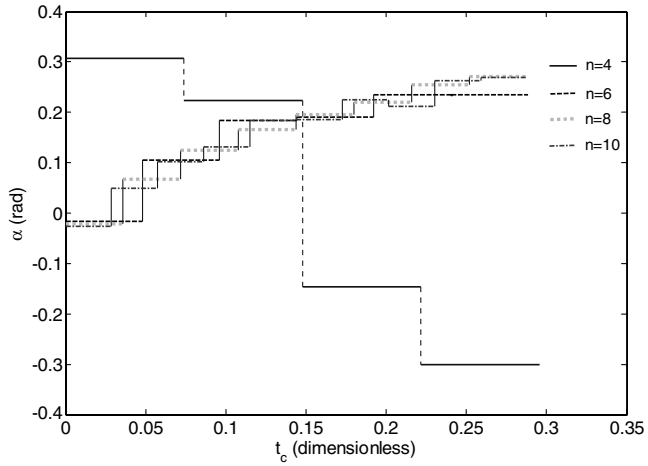

Fig. 12 Control law of E-A-II transfer trajectories minimizing t_c.

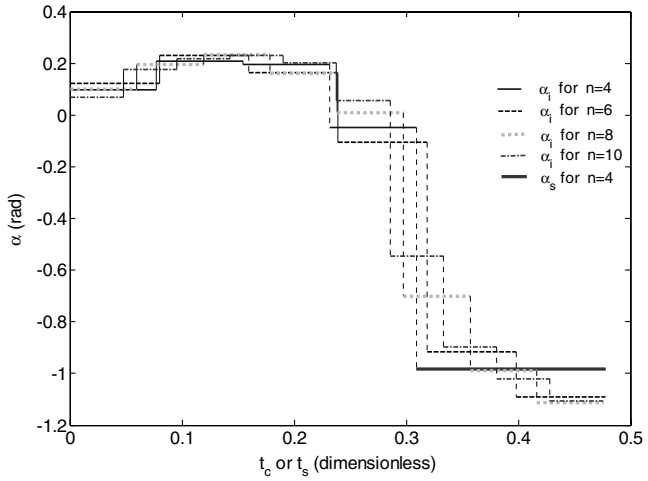

Fig. 13 Control law of E-A-II transfer trajectories minimizing $t_c + t_s$.

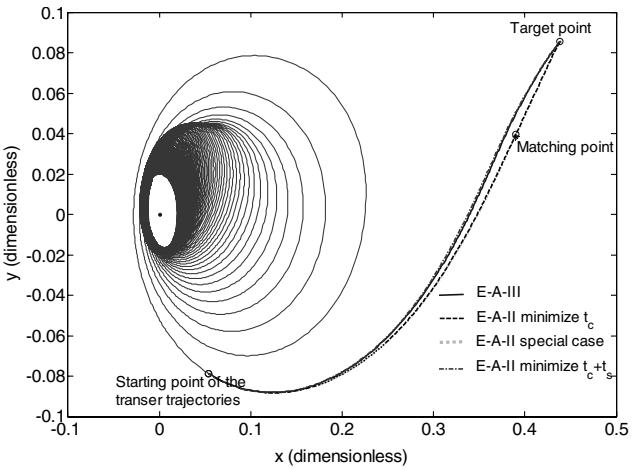

a) Transfer trajectory

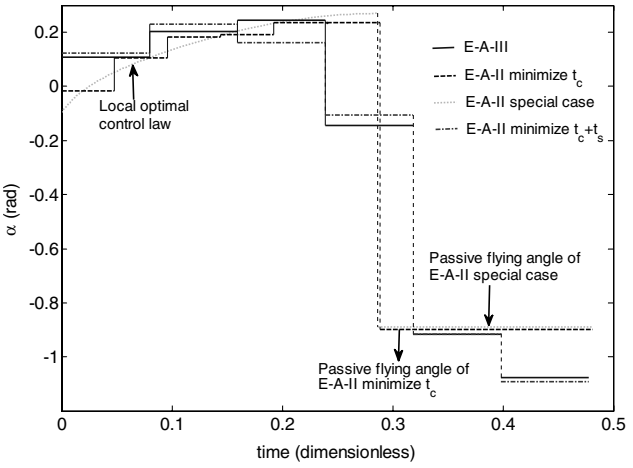

b) Control law

Fig. 14 Comparison between different transfer trajectories.

achieved using direct method [9]. The results show that the transfer time is almost independent of the number of segments, decreases very slowly as the number increases. It means that only a small number will generate a near minimum-time result. For example, the transfer time difference between 4-segment and 10-segment transfer trajectories is about several hours. The cone angle history shows that the angle increases slowly at the beginning of the journey and decreases steeply at the end of the journal.

For E-A-II transfer trajectories minimizing t_c, the active control time is almost independent of the number of segments. The difference of active control time between 4-segment and 10-segment trajectories is about several hours. However, the number of segments influences the total transfer time greatly. For transfer trajectories whose segments are less than 5, the total transfer time is much larger. As shown in Fig. 12, for a typical 4-segment trajectory, the stable manifold of the target point circles around the Earth for a loop before arrival at the target point. The transfer trajectories whose segments are more than 5 are very similar. A typical 6-segment transfer trajectory can be described as follows: after escape, it takes 0.2886 dimensionless time (16.7766 days) to control the sail entering the passive flying stage. Then, the sail flies along the stable manifold with a cone angle of -0.8990 rad, and arrives at the target point in 0.1924 dimensionless time (11.1844 days).

For E-A-II transfer trajectories minimizing$t_c + t_s$, similarly, the transfer time is almost dependent of the number of segments. The increase of the number of segments generates a very small reduction in transfer time. The transfer trajectory converges to an E-A-III transfer trajectory when the number of segments is more than 4, which means that the passive flying time tends to zero.

From above results we know that the parameters of the transfer trajectories are almost independent of the number of segments when it is larger than 5. Therefore, different cases of 6-segment transfer trajectories are compared with the E-A-II special transfer trajectory, as shown in Fig. 14. The following conclusions can be drawn:

1) The total transfer time of different transfer trajectories is insensitive to different objective functions. The total transfer time is close and the differences between different transfer trajectories are several hours.

2) The active control time of E-A-II special case and E-A-II minimizing t_c is the smallest among all cases. These two kinds of transfer trajectories are similar in terms of both total transfer time and active control time. The difference is that E-A-II uses a continuous control law, while E-A-II minimizing t_c uses a discrete control law during the active control stage.

3) The E-A-II special case generates a near minimum-time transfer trajectory, though the transfer time is not optimized. It means that the local optimal control law is still a good approximation to a minimum-time control law.

4) The passive flying time of E-A-II minimizing $t_c + t_s$ converges to zero. It means that E-A-II minimizing $t_c + t_s$ is equivalent to an E-A-III transfer trajectory.

5) From the comparison results, we know that the total transfer time is close for all transfer trajectories. Therefore, the transfer trajectory including the longest passive flying time is favorable. The E-A-II minimizing t_c is one of these transfer trajectories.

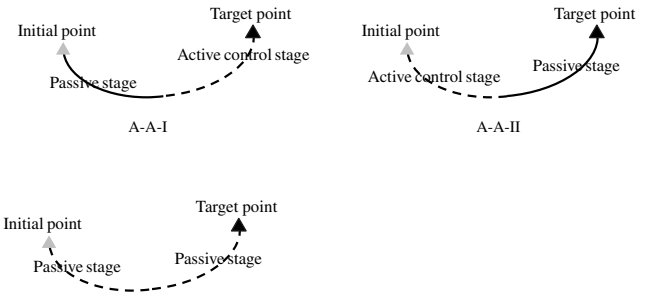

Fig. 15 Illustrations of three different A-A transfer trajectories.

Table 3 Design parameters for A-A-I and A-A-II cases

Design parameters	A-A-II	A-A-I
Active control time, day	30.70353	67.82602
Passive flying time, day	190.71881	156.82814
Passive cone angle, rad	1.01648	−1.32465
Position error, m	1.98505	0.32485
Velocity error, m/s	3.03708e − 7	2.07381e − 6

B. A-A Transfer Trajectories (Artificial Lagrange Points to Artificial Lagrange Points)

For the transfer trajectories between equilibrium points, no chemical propulsion is used. The invariant manifolds of both initial and target points are used to design the transfer trajectories. There are three kinds of different transfer trajectories, as shown in Fig. 15.

1) A-A-I: The sail departs from the initial point along its unstable manifold. The active control is triggered at the end of the passive stage. Then, the attitude is adjusted to make the sail arrive at the target point.

2) A-A-II: The sail is controlled to enter the stable manifold of the target point. The sail flies to the target point along its stable manifold with a fixed cone angle.

3) A-A-III: There is no active control stage for the A-A-III transfer trajectory. The sail departs from the initial point along the unstable manifold and flies to the target point along the stable manifold. One stable manifold of the initial point matches one unstable manifold of the target point at a point.

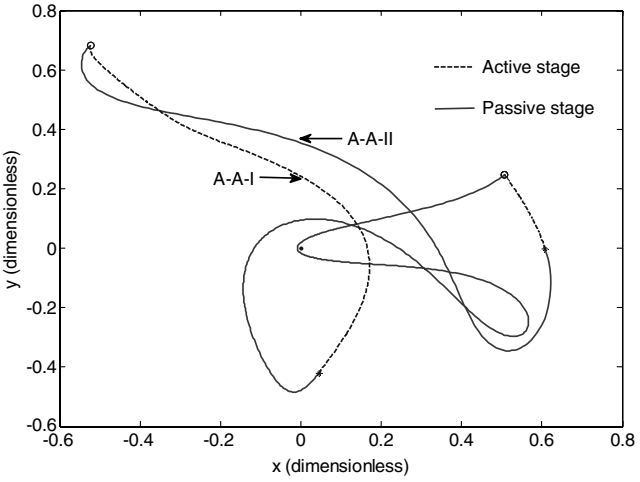

a) Transfer trajectory

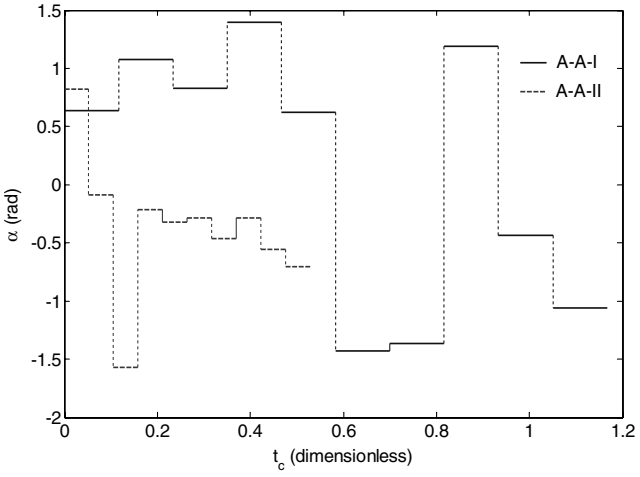

b) Active control law

Fig. 16 Transfer trajectory and control law for active control.

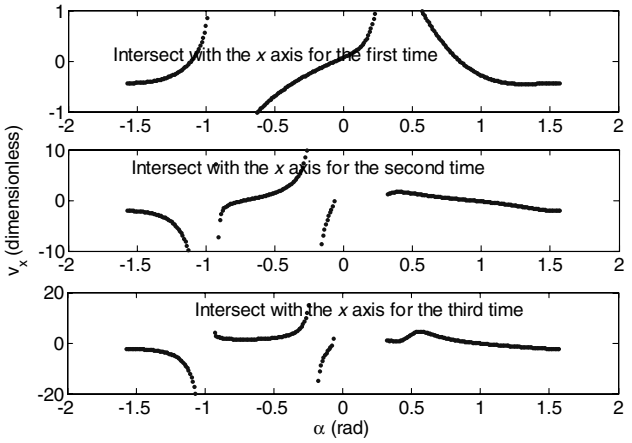

a) Panoramagram of v_x

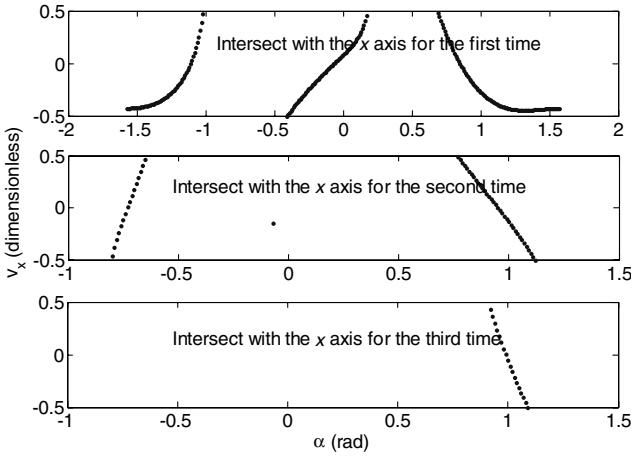

b) Passing through zero regions with enlarged scale

Fig. 17 The velocity along the *x* axis at the intersection point.

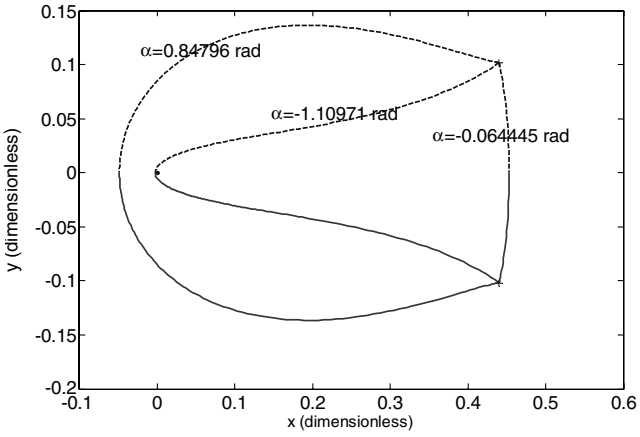

a) Trajectories for transfer *1*

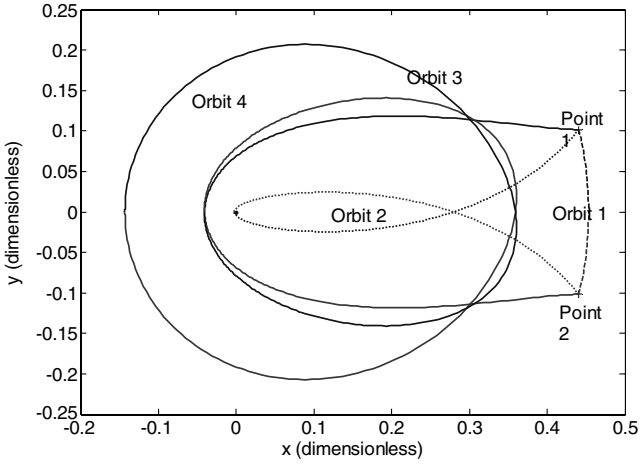

b) Trajectories for transfers *1*, *2* and *3*

Fig. 18 Symmetrical transfer trajectories between symmetrical points.

1. A-A I and A-A II Transfer Trajectory Design

Both A-A-I and A-A-II transfer trajectories include an active control and a passive flying stage. The transfer trajectories minimizing the active control time are discussed. Similarly, the design problem is converted into a parameter optimization problem. The active control stage is discretized into n segments. During each segment, the cone angle is fixed constant, $\alpha_i (i = 1 \ldots n)$, and the time span of this stage is t_c. The passive flying stage has two parameters: the passive cone angle α_p and flying time t_p. For A-A-I transfer, the passive flying stage is integrated backward in time. The final states of the two stages match at some point on the stable manifold of the target point. The defect of the two states at the matching point being zero is the constraint. For A-A-II transfer, the whole trajectory is integrated forward in time and the state error of the sail at the target point being zero is the constraint. For both cases, the optimization parameters of the problem are given by

$$Y = [\alpha_1 \quad \ldots \quad \alpha_n \quad t_c \quad \alpha_p \quad t_p]^T \tag{48}$$

The constraint of the problem is given by

$$\boldsymbol{\Phi}(\boldsymbol{Y}) = 0 \tag{49}$$

The objective function is chosen to be the time span of the active control stage, which is given by

$$F_{\text{obj}} = t_c \tag{50}$$

Similarly, the optimization problem is converted into an unconstrained optimization problem by introducing the Lagrange multiplier.

A solar sail of $a_0 = 4(0.3416\ \text{mm/s}^2)$ can equilibrate at points $\boldsymbol{r}_1 = [0.506197 \quad 0.246217]^T$ and $\boldsymbol{r}_2 = [-0.523499 \quad 0.682477]^T$ with different cone angles. Both A-A-I and A-A-II transfer trajectories from $\boldsymbol{r}_1$ to $\boldsymbol{r}_2$ are designed here. Table 3 gives the values of the optimized parameters. The whole transfer trajectory and active control law are given in Figs. 16a and 16b, respectively.

From the optimization results we find that the total transfer time of the two cases is very close. The active control time of A-A-II is much shorter than that of A-A-I. Therefore, A-A-II transfer trajectory takes advantages over A-A-I transfer trajectory with respect to minimizing active control time. For engineering practice, the active control is always necessary because of all kinds of perturbations and model

Table 4 Parameters for transfer 1

Orbit number	Cone angle for unstable manifold, rad	Flying time for unstable manifold, day
1	−0.064445	23.71203
2	−1.10971	22.00428
3	0.84796	28.91660

Table 5 Parameters for transfers 1, 2, and 3

Orbit number	Cone angle for unstable manifold, rad	Flying time for unstable manifold, day
1	−0.064445	23.71203
2	−0.73157	24.74478
3	0.98922	73.19220

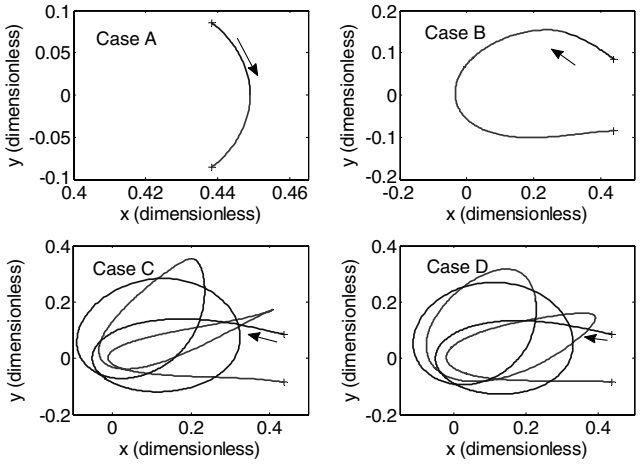

Fig. 19 Different transfer trajectories between two points.

errors. In this point of view, A-A-I is more practical than A-A-II because the errors caused by passive flying stage can be corrected during the active control stage.

2. A-A-III Transfer Trajectory Design

In this section, the transfer trajectories including two passive stages are investigated. The unstable manifolds of the initial point and stable manifolds of the target point are matched to form transfer trajectories. The sail departs from the initial point along the unstable manifold and enters the stable manifold of the target point directly at the end of the unstable manifold stage.

a. Symmetrical Transfer Trajectories Between Symmetrical Points. In Hill's restricted three-body problem, if $(x \quad y \quad \dot{x} \quad \dot{y} \quad t \quad \alpha)$ is one solution to the dynamical equations, the symmetrical solution with respect to the x axis $(x \quad -y \quad -\dot{x} \quad \dot{y} \quad -t \quad -\alpha)$ exists. According to this symmetry, the symmetrical transfer trajectories between symmetrical points can be developed. Symmetrical points $[x_0 \quad y_0]$ and $[x_0 \quad -y_0]$ are of the same requirement on the solar sail characteristic acceleration. The stable manifolds of $[x_0 \quad y_0]$ and unstable manifolds of $[x_0 \quad -y_0]$ are symmetrical with respect to the x axis and vice versa. In addition, the trajectory of a solar sail departing from $[x_0 \quad y_0]$ with a cone angle α_0 and the trajectory of a sail from $[x_0 \quad -y_0]$ with angle $-\alpha_0$ going backward in time are symmetrical with respect to the x axis. If one trajectory has an intersection point with the x axis, the other will have the same intersection point with the x axis. Further, if the velocity of the sail along the x axis is zero, the velocities of the symmetrical trajectories coincide with each other at the intersection point and the two symmetrical trajectories are therefore matched smoothly. Thus, the trajectory design is to find a passive flying segment that has a zero velocity along the x axis when passing the x axis.

When the manifolds are globalized, the cone angle is regarded as a free parameter. Taking $y = 0$ as a Poincare section, the relation between the cone angle and the velocity along the x axis on the Poincare section can be obtained. For some cone angles, the manifolds may intersect with the Poincare section several times. To separate the transfer trajectories that intersect with the Poincare section for different times, the trajectory intersecting the Poincare section for the nth time during one passive flying stage is labeled as transfer n. If there are k trajectories of transfer n, they are labeled as transfer n_i $(i = 1 \ldots k)$, respectively.

Figure 17 shows the cone angle and velocity along the x axis on the Poincare section, where 17a gives the panoramagram of the intersection parameters. It shows that the trajectory has at least one intersection point with the x axis when the sail flies with different cone angles. The sail intersects with the x axis for the second and third times for most cone angles. Figure 17b shows the local regions where v_x passes through zero. For transfer 1, three cone angles exist for passing through the Poincare section with a zero velocity along the x axis, two angles for transfer 2, and one angle for transfer 3. The simulation shows that transfers 4 and 5 also exist. The method of bisection will find the passing-zero point. The trajectories of transfers 1_1, 1_2, and 1_3 are shown in Fig. 18a and the corresponding transfer parameters are given in Table 4. The transfer time of three trajectories is close, though the distances of travel are greatly different. Orbit 1_1 is the shortest in distance of travel, but the travel time is longer than that of orbit 1_2. As discussed above, the cone angle has to be adjusted from the current value to its counterpart at the intersection point to make the sail enter the second passive flying stage. The quantity of the attitude adjustment increases with absolute value of the cone angle. Consequently, orbit 1_1 is superior to the others with the consideration of attitude adjustment. Figure 18b shows the transfer trajectories intersecting with the x axis for different numbers of times. The corresponding parameters are given in Table 5. The transfer times of orbits 1 and 2 are close, and the time of orbit 3 is much longer, because the sail circles around the Earth for about three loops. This kind of transfer orbit can be used to collect data or send data in the vicinity of the Earth before or after working at the artificial Lagrange point.

b. Passive Transfer Trajectories for General Cases. The symmetrical transfer trajectories are obtained by checking the symmetry of the dynamical equation. This section investigates the transfer trajectories for general cases. Similarly, the whole transfer trajectory is divided into two passive flying stages. The stable manifold of the initial point and unstable manifold of the target point are matched at some point that may not be on the x axis, which is different from the symmetrical trajectory. It is difficult to prove the existence of the solution or how many solutions exist. We can only use the numerical method to check if the solution exists. The parameter optimization method is employed here to obtain the transfer trajectory. For each passive flying stage, the cone angle and flying time can be optimized. Therefore, the optimization parameters can be given by

$$\boldsymbol{Y} = [t_s \quad \alpha_s \quad t_u \quad \alpha_u]^T \tag{51}$$

The stable manifold stage is integrated backward in time and the final states of the two stages are matched at some point. Therefore, the position and velocity errors at the matching point are optimized to be minimal. The optimization object function is given by

$$F_{\text{obj}} = \boldsymbol{\lambda}^T \boldsymbol{\Phi}(Y) + \frac{1}{2} c |\boldsymbol{\Phi}(Y)|^2 \tag{52}$$

If the optimal result is zero, the transfer trajectory between two points exists. If we can not find a solution, strictly speaking, it can not be concluded that the solution does not exist. More important, the problem is dependent on the mission transfer trajectory. No solution exists for some transfer trajectories, while multisolutions exists for others. We know that the transfer trajectories between two symmetrical points exist (at least a symmetrical transfer trajectory).

Table 6 Parameters for different transfer trajectories between two points

Case	Cone angle for unstable manifold, rad	Cone angle for stable manifold, rad	Flying time for unstable manifold, day	Flying time for stable manifold, day
A	-0.017991	0.018010	25.31118	25.31118
B	0.57506	-1.07935	25.40159	34.69829
C	0.77787	1.39524	107.51209	83.98453
D	0.82263	-1.30536	92.58937	89.62505

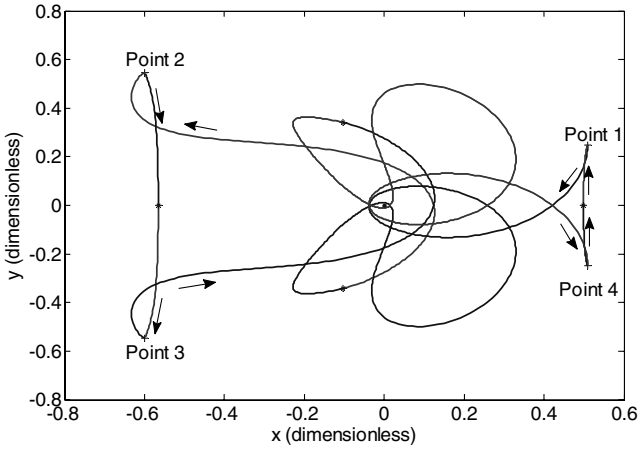

Fig. 20 Trajectory of a tour mission around the Earth.

Here, an example of the transfer trajectories between two symmetrical points is given. In the simulation results, if the errors can be reduced below the specified tolerance, the obtained trajectory is regarded as the transfer trajectory. The position tolerance is set to 10 m and the velocity tolerance is 0.1 mm/s.

The characteristic acceleration of the solar sail is $a_0 = 4$ (0.3416 mm/s^2), and the transfer trajectories between different points are designed to have the same characteristic acceleration requirement on the sail. In simulation for transfer trajectories between symmetrical points, the initial and target points are determined by $x_0 = 0.43818$ and are symmetrical with respect to the x axis. Different transfer trajectories with different flying times are shown in Fig. 19. The trajectory of case A is a symmetrical one that can be obtained according to the symmetry of the equation, and the others are unsymmetrical transfers. The trajectory of case B looks like a symmetrical one and the parameters in Table 6 show that both the cone angle and time are unsymmetrical. The trajectories of cases C and D are very similar, and both circle around the Earth for several loops. The transfer time is much longer for the two cases. It can be found that circling around the Earth for one loop takes about 0.4 dimensionless time (23.25 days).

3. Tour Mission Design

It can be found from Fig. 2 that a solar sail can be equilibrated at different points. It is possible for a sail to work at different points that have the same requirement on the sail characteristic acceleration. A tour mission around the Earth is designed: the sail works at an artificial Lagrange point in the first quadrant in the xy plane for some time; then it travels to a point in the second quadrant for another mission, and then it travels to a point in the third quadrant after the mission at point 2. Finally, it travels to point 4 in the fourth quadrant and returns to the initial point 1, as shown in Fig. 20. In this tour mission, the sail travels around the Earth for several loops and works at four different places in each direction with respect to the sun–Earth line. In this mission design, both the symmetrical and unsymmetrical transfer trajectories are adopted here. The transfer trajectories from points 2–3 and from points 4–1 are symmetrical trajectories between symmetrical points. The trajectories of points 1–2 and 3–4 are unsymmetrical ones obtained by the optimization method. The two trajectories are symmetrical with respect to the x axis, where the unstable manifold of point 4 and the stable manifold of point 1 are symmetrical, and the stable manifold of point 2 and the unstable manifold of point 3 are symmetrical. Consequently, the whole transfer trajectory is symmetrical with respect to the sun–Earth line. The transfer time and cone angles for each segment are given in Table 7.

Different transfer trajectories have been described above. The common aspect of different transfer trajectories is that the manifold of the artificial Lagrange point is used for each case. The difference is whether active control or impulse is required during the transfer journey. These transfer trajectories can be regarded as reference trajectories for certain missions. Transfer trajectories from Earth orbits to artificial Lagrange points can be used for a solar sail demonstration mission. This kind of trajectory is suitable for solar sail demonstration because the sail flies passively and no active control is required during the transfer journey. The sail is deployed after being inserted into the stable manifold of an equilibrium point. During the journey, the solar radiation pressure force can be tested. If the sail arrives at the target point successfully, the active control of the solar sail can be tested using the transfer trajectories between different points. As we know, active control is always a challenge for solar sails. Because these transfer trajectories require a short active control time, they are also useful because the solar sail technology is mature for application.

V. Conclusions

In this paper, a new concept of invariant manifolds associated with solar sails is proposed. For artificial Lagrange points in the vicinity of the Earth, one stable manifold and one unstable manifold exist. The invariant manifolds were used to design transfer trajectories. For transfer trajectories from Earth orbits to the equilibrium points, three kinds of trajectories are investigated. For transfer trajectories requiring impulses, the energy is calculated and compared with that required by a transfer using chemical propulsion. Tens to hundreds of meters-per-second velocity increments can be saved depending on target points. For transfer trajectories without impulses, different objective functions are used to design the transfer trajectories. The comparison of different results shows that the total transfer time is insensitive to the objective functions. For the transfer trajectories between artificial Lagrange points, three different transfer trajectories were investigated. The transfer time of the active stage is minimized using a direct shooting method. The active stage can be removed for some special cases. The whole transfer trajectory consists of two passive stages. These kinds of transfer trajectories can be obtained by an optimization method. In particular, symmetrical transfer trajectories with respect to the sun–Earth line between symmetrical points are obtained using the symmetry of the dynamical system.

Acknowledgments

This work was supported by the National Natural Science Foundation of China (Grants No.10902056 and No. 10832004). The authors would like to acknowledge D. Christopher, Tsinghua University, for meticulous revision for the paper.

References

[1] Tsu, T. C., "Interplanetary Travel by Solar Sail," *American Rocket Society*, Vol. 29, 1959, pp. 422–427.

[2] Koblik, V. V., "Controlled Solar Sailing Transfer Flights into Near-Sun Orbits under Restrictions on Sail Temperature," *Cosmic Research*

Table 7 Transfer parameters for the tour around the Earth

Segment	Cone angle for unstable manifold, rad	Cone angle for stable manifold, rad	Flying time for unstable manifold, day	Flying time for stable manifold, day
Point 1 to point 2	−0.75191	1.08691	133.22473	122.66813
Points 2 to point 3	−0.74422	0.74422	37.33176	37.33176
Point 3 to point 4	−1.08691	0.75191	122.66813	133.22473
Point 4 to point 1	0.95632	−0.95632	26.58333	26.58333

(Translation of Kosmicheskie Issledovaniya), Vol. 34, 1996, pp. 572–578.

[3] Zhukov, A. N., and Lebedev, V. N., "Variational Problem of Transfer Between Heliocentric Circular Orbits by Means of a Solar Sail," *Cosmic Research (Translation of Kosmicheskie Issledovaniya)*, Vol. 2, 1964, pp. 41–44.

[4] Sauer, C. G., "Optimum Solar Sail Interplanetary Trajectories," *AAS/AIAA Astrodynamics Conference*, AIAA, New York, 1976, pp. 76–792.

[5] Sackett, L. L., and Edelbaum, T. N., "Optimal Solar Sail Spiral to Escape," *AAS/AIAA Astrodynamics Conference*, AIAA, New York, 1977, pp. 34–38.

[6] Subba Rao, P. V., and Ramanant, R. V., "Optimum Rendezvous Transfer Between Coplanar Heliocentric Elliptic Orbits Using Solar Sail," *Journal of Guidance, Control, and Dynamics*, Vol. 15, No. 6, 1992, pp. 1507–1509. doi:10.2514/3.11417

[7] Simon, K., and Zakharov, Y., "Optimization of Interplanetary Trajectories with Solar Sail," *46th International Astronautical Federation Congress*, International Astronautical Federation Paper 95-A.2.08, Oct. 1995.

[8] Jayarman, T. S., "Time-Optimal Orbit Transfer Trajectory for Solar Sail Spacecraft," *Journal of Guidance, Control, and Dynamics*, Vol. 3, No. 6, 1980, pp. 536–542. doi:10.2514/3.19723

[9] Otten, M., and McInnes, C. R., "Near Minimum-Time Trajectories for Solar Sails," *Journal of Guidance, Control, and Dynamics*, Vol. 24, No. 3, 2001, pp. 632–634. doi:10.2514/2.4758

[10] Dachwald, B., "Optimization of Interplanetary Solar Sailcraft Trajectories Using Evolutionary Neurocontrol," *Journal of Guidance, Control, and Dynamics*, Vol. 27, No. 1, 2004, pp. 66–72. doi:10.2514/1.9286

[11] Fekete, T. A., "Trajectory Design for Solar Sailing from Low-Earth Orbit to the Moon," *AAS/AIAA Spaceflight Mechanics Meeting*, AAS Paper 92-184, 1992.

[12] Coverstone, V. L., and Prussing, J. E., "Technique for Escape from Geosynchronous Transfer Orbit Using a Solar Sail," *Journal of Guidance, Control, and Dynamics*, Vol. 26, No. 4, 2003, pp. 628–634. doi:10.2514/2.5091

[13] Mengali, G., and Quarta, A. A., "Earth Escape by Ideal Sail and Solar-Photon Thruster Spacecraft," *Journal of Guidance, Control, and Dynamics*, Vol. 27, No. 6, 2004, pp. 1105–1108. doi:10.2514/1.10637

[14] Macdonald, M., and McInnes, C. R., "Realistic Earth Escape Strategies for Solar Sailing," *Journal of Guidance, Control, and Dynamics*, Vol. 28, No. 2, 2004, pp. 315–323.

[15] Green, A. J., "Optimal Escape Trajectory from a High Earth Orbit by Use of Solar Radiation Pressure," Master of Science Thesis, Cambridge, Massachusetts Institute of Technology, 1977.

[16] McInnes, C. R., Simmons, J. F. L., and MacDonald, E. W., "Solar Sail Parking in Restricted Three-Body System," *Journal of Guidance, Control, and Dynamics*, Vol. 17, No. 2, 1994, pp. 399–406. doi:10.2514/3.21211

[17] West, J. L., and Derbes, B., "Solar Sail Vehicle System Design for the Geostorm Warning Mission," *AIAA Space 2000 Conference*, AIAA 2000-5326, 2000.

[18] West, J. L., "The Geostorm Warning Mission: Enhanced Opportunities Based on New Technology," *14th AAS/AIAA Space Flight Mechanics Conference*, AAS Paper 04-102, 2004.

[19] Simmons, J.F.L., McDonald, A.J.C., and Brown, J. C., "The Restricted 3-Body Problem with Radiation Pressure," *Celestial Mechanics and Dynamical Astronomy*, Vol. 35, No. 2, 1985, pp. 145–187.

[20] Bookless, J., and McInnes, C. R., "Control of Lagrange Point Orbits Using Solar Sail Propulsion," *Acta Astronautica*, Vol. 62, Nos. 2-3, 2008, pp. 159–176. doi:10.1016/j.actaastro.2006.12.051

[21] Bookless, J., and McInnes, C. R., "Dynamics and Control of Displaced Periodic Orbits Using Solar-Sail Propulsion," *Journal of Guidance, Control, and Dynamics*, Vol. 29, No. 3, 2006, pp. 527–537. doi:10.2514/1.15655

[22] Baoyin, H., and McInnes, C. R., "Solar Sail Equilibria in the Elliptical Restricted Three-Body Problem," *Journal of Guidance, Control, and Dynamics*, Vol. 29, No. 3, 2006, pp. 538–542. doi:10.2514/1.15596

[23] McInnes, C. R.,"Passive Control of Displaced Solar Sail Orbits," *Journal of Guidance, Control, and Dynamics*, Vol. 21, No. 6, 1998, pp. 975–982. doi:10.2514/2.4334

[24] Gong, S. P., Li, J. F., and Baoyin, H., "Passive Stability Design for the Solar Sail on Displaced Orbits," *Journal of Spacecraft and Rockets*, Vol. 44, No. 5, 2007, pp. 1071–1079. doi:10.2514/1.29752

[25] Kirpichnikov, S. N., Polyakhova, E. N., and Shmyrov, A. S., "Planar Heliocentric Roto-Translatory Motion of a Spacecraft with a Solar Sail of Complex Shape," *Celestial Mechanics and Dynamical Astronomy*, Vol. 63, Nos. 3-4, 1996, pp. 255–269. doi:10.1007/BF00692290

[26] Van de Kolk, C. B., "Orbital Aspects of a Two-Plane Solar Sail," *AIAA Space Technology Conference and Exposition-1999*, AIAA Paper 99-4489.

[27] Van de Kolk, C. B., "Complex Shaped Solar Sails: A Study of the Coupled Attitude and Trajectory Dynamics," Ph.D. Dissertation, Dept. of Aerospace Engineering, Univ. of Tennessee, Knoxville, TN, 2000.

[28] Waters, T. J., and McInnes, C. R., "Periodic Orbits Above the Ecliptic in the Solar-Sail Restricted Three-Body Problem, " *Journal of Guidance, Control, and Dynamics*, Vol. 30, No. 3, 2007, pp. 687–693. doi:10.2514/1.26232

[29] Gomez, G., Jorba, A., Masdemont, J., and Simo, C., "Study of the Transfer from the Earth to a Halo Orbit Around the Equilibrium Point L1," *Celestial Mechanics and Dynamical Astronomy*, Vol. 56, No. 4, 1993, pp. 541–562. doi:10.1007/BF00696185

[30] Waters, T. J., and McInnes, C. R., "Invariant Manifolds and Orbit Control in the Solar Sail Three-Body Problem," *Journal of Guidance, Control and Dynamics*, Vol. 31, No. 3, 2008, pp. 554–562. doi:10.2514/1.32292

[31] McInnes, C. R., *Solar Sailing. Technology Dynamics and Mission Applications*, Springer–Verlag, London, 1999, pp. 136–140.